ACS APPLIED MATERIALS & INTERFACES

Research Article

www.acsami.org

Optically Transparent Cathode for Co(III/II) Mediated Dye-Sensitized Solar Cells Based on Graphene Oxide

Ladislav Kavan,*[,†,‡] Jun-Ho Yum,[†] and Michael Graetzel[†]

[†]Laboratory of Photonics and Interfaces, Institute of Chemical Sciences and Engineering, Swiss Federal Institute of Technology, CH-1015 Lausanne, Switzerland

[‡]J. Heyrovský Institute of Physical Chemistry, v.v.i., Academy of Sciences of the Czech Republic, Dolejškova 3, CZ-18223 Prague 8, Czech Republic

Supporting Information

ABSTRACT: Thin semitransparent films were fabricated on F-doped SnO_2 (FTO) from single-layer graphene oxide (GO) either pure or in a composite with graphene nanoplatelets. Electrocatalytic activity of prepared films was tested for the $Co(bpy)_3^{3+/2+}$ redox couple in acetonitrile electrolyte solution. Pristine GO showed almost no activity, resembling the properties of basal plane pyrolytic graphite. However, electrochemical performance of graphene oxide improved dramatically upon chemical reduction with hydrazine and/or heat treatment. All GO-containing films were firmly bonded to FTO, which contrasted with the poor adhesion of sole graphene nanoplatelets to this support. The activity loss during long-term aging was considerably improved, too. Enhanced stability of GO-containing films together with high electrocatalytic activity is beneficial for application in a new generation of dye-sensitized solar cells employing $Co(bpy)_3^{3+/2+}$ as the redox shuttle.

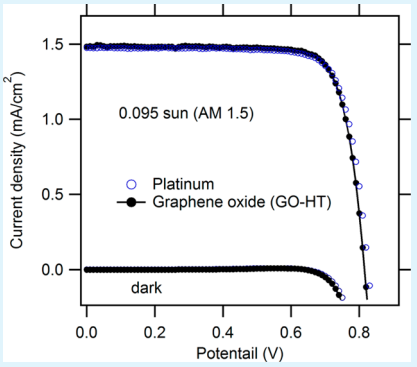

KEYWORDS: *graphene oxide, reduced graphene oxide, dye sensitized solar cell, cobalt redox shuttle, electrochemical impedance spectroscopy*

1. INTRODUCTION

The dye-sensitized solar cell (DSC) also called the Graetzel cell is alternative to Si-based photovoltaics, offering comparable efficiency at lower cost and easier fabrication.[1−5] Until recently, DSC electrode materials used noble metals (Ru-dyes, Pt catalyst) and the low cost of DSC stemmed from small amounts of precious metals applied in actual devices. Traditional liquid-junction DSC employs the I_3^-/I^- redox mediator, which transports holes from a photooxidized dye (adsorbed on the TiO_2 photoanode) through the electrolyte solution towards the counterelectrode made from platinized F-doped SnO_2 (FTO). Due to small amounts of Pt used (ca. 10 $\mu g/cm^2$) this counterelectrode is optically transparent which is beneficial for certain practical applications, albeit not mandatory for proper function of DSC.[4,6] The electrocatalytic activity of Pt was thought to be unique for the I_3^-/I^- redox reaction,[7,8] but recently Gong et al.[6] discovered that $Co_{0.85}Se$ exhibited significantly higher activity for this redox pair, and their DSC with $Co_{0.85}Se$-FTO cathode performed better than that with the Pt-FTO cathode.

Nevertheless, the I_3^-/I^- system is hardly the optimum mediator for DSC because of its low redox potential (ca. 0.35 V vs. SHE) which limits the accessible open-circuit voltage (V_{OC}) of DSC.[4,7,9,10] Among other possible redox shuttles[7,10] the Co-polypyridine complexes coupled with donor-bridge-acceptor sensitizers, turned out to be particularly promising.[4,9−20] Thus, the redox potential of $Co(bpy)_3^{3+}/Co(bpy)_3^{2+}$ (bpy is 2,2′-bipyridine) equals 0.56 V vs. SHE, and this redox shuttle provided solar cells with V_{OC} near 0.9 V.[4,9−11,13,18] The $Co(bpy)_3^{3+}/Co(bpy)_3^{2+}$ redox mediator in conjunction with an optimized combination of dyes as sensitizers demonstrated DSC with power conversion efficiency of 12.3% which is the current world record of DSC performance.[18]

Most Co-mediated solar cells, including the champion (12.3 %)-cell[18] still rely on Pt-FTO cathode[13−18,21] and occasionally also conducting polymers (PEDOT or PProDOT) were used with interesting results.[11,12,17] The application of carbon as a cathode catalyst in Co-mediated DSC was pioneered by Sapp et al.[21] already in 2002. Their carbon cathode initially outperformed platinum, but was unstable.[21] In contrast, screen-printed carbon was less active than platinum for redox reaction of tris(4,4′-di-tertbutyl-2,2′-bipyridine)cobalt(III/II).[22]

Graphene-based materials, viz. functionalized graphene sheets (FGS) were introduced for iodide-mediated DSC by Roy-Mayhew et al.[23] The catalytic activity of FGS correlated with the amount of oxygen in carbonaceous skeleton, until certain limit when the electrical conductivity became performance-controlling.[23] This work further stressed the role of Nernst diffusion impedance in the pores of carbon film.[23] It can be neglected only in thin films, e.g., from graphene nano-

Received: October 8, 2012
Accepted: November 20, 2012
Published: November 26, 2012

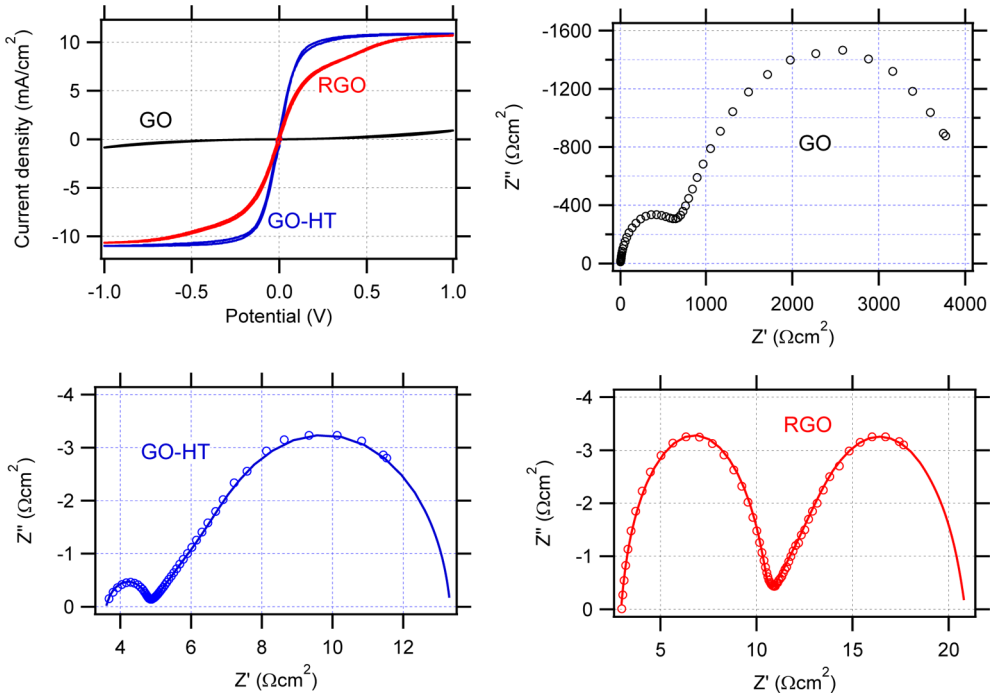

Figure 1. Electrochemical activity of FTO supported thin films from graphene oxide (GO), reduced graphene oxide (RGO) and heat-treated graphene oxide (GO-HT). The electrocatalytic activity was tested on symmetrical dummy cells. Top-left: Cyclic voltammogram, scan rate 10 mV/s. The remaining charts show Nyquist plots of electrochemical impedance spectra measured at 0 V from 65 kHz to 0.1 Hz.

platelets (GNP), which may be even optically transparent, although their catalytic activity for I_3^-/I^- redox pair is less good.[24] The follow up studies of graphene cathode for I-mediated DSC essentially confirmed that performance comparable to Pt is hard to achieve.[25−33]

Surprisingly, the same optically transparent GNP electrode, which was sluggish for I-mediated DSC[24] turned out to be highly active for Co-mediated DSC, using $Co(bpy)_3^{3+/2+}$ redox couple[19] or $[Co(bpy\text{-}pz)_2]^{3+/2+}$; bpy-pz is 6-(1H-pyrazol-1-yl) 2,2′-bipyridine.[20] Similarly, the porous FGS electrode, containing residues of partly pyrolyzed ethylcellulose, exhibited excellent performance in $Co(bpy)_3^{3+/2+}$ mediated DSC too.[26] However, this initial success of graphene-based cathode in Co-mediated DSC[19,20,24,26] left several fundamental and technical issues to be addressed. The basic unanswered question is, where the catalytic activity of carbon materials for Co(III)/(II) (and also for I_3^-/I^-) redox reactions comes from? This problem is usually bypassed by a hypothesis that "defects" and "oxygen-containing groups" are the catalytically active sites, but they were never clearly identified. In general, electrocatalysis through carbon−oxygen surface functionalities is a contradictory subject with many opposing claims.[34] Roy-Mahew at al.[23] proposed that carbons for DSC cathode could be optimized by enhancement of the amount of specific catalytic sites, and by elimination of inactive defects, if they were known.

Another unanswered, but presumably related question, is the loss of activity in Co-mediated systems, first reported by Sapp et al.[21] for carbon cathode and reproduced by ourselves[19,20] for aged (days) optically transparent GNP electrode. This aging is virtually similar to 'poisoning' of Pt[6,24,35] or metal selenides[6] in I-mediated systems, but the chemistry behind poisoning is unknown in all cases.[6,19,20,24,35] Among the technical problems to be solved for transparent GNP electrodes, is the poor adhesion of graphene nanoplatelets to FTO.[19,20,24] The active layer is mechanically unstable, hence nanoplatelets detaching from the support may be responsible for higher dark current in DSC, and thus for lower open-circuit voltage.[26]

This work is addressing some of the mentioned open problems. Here, we report on the improvement of fabrication protocol toward optically transparent graphene-based layers, yielding wear-resistant films with good adhesion to FTO. In this way, we succeeded in decreasing the dark current in DSC and stability against aging, but we kept the good electrocatalytic activity at the same time. Also we collected here new facts towards ongoing discussion of electrocatalytic sites in carbons.

2. RESULTS AND DISCUSSION

Graphene nanoplatelets (GNP) which have been investigated in our earlier works,[19,20,24] are insoluble in any solvent and do not adhere well to FTO upon deposition from liquid dispersions. Both problems are avoided with single-layer graphene oxide (GO) used in this work. This material is soluble in water, and also the mixed aqueous solutions of GO/GNP (see the Experimental Section) do not flocculate during, at least, weeks at room temperature. The amphiphilic character of GO stems from the presence of large amount of oxidic functional groups on the condensed aromatic backbone. Therefore, GO is known to act as surfactant to solubilize carbon nanotubes and nanotubes/fullerene-C_{60} mixtures in water.[36] We assume that surfactant-aided solubilization occurs also in our GO/GNP mixture. Furthermore, the solution-processable films deposited on FTO glass from GO or GO/GNP mixtures, are robust and wear resistant. Their mechanical stability against, for example, wiping with tissue is much better compared to films from pure GNP. The strong attachment of GO-based films to FTO is probably caused by intimate interaction of hydrophilic functionalities in GO with hydroxylated surface of FTO. In our optically transparent cathodes, the amount of carbonaceous material is very low (typically ca. 0.3 to 10 $\mu g/cm^2$).[19] Such small amounts of carbon are difficult to

quantify accurately as mass or layer thickness. However, the optical density of carbonaceous film is a useful quantitative parameter for carbon loading in actual electrodes. To this purpose, we adopt the usual convention that the film is characterized by its optical transmittance at a wavelength of 550 nm (T_{550}, see Experimental Section for details).[19,20,24]

The electrocatalytic performance of DSC-cathodes was tested using symmetrical dummy cells.[6,19,20,23,24,26] Herein, a thin layer of electrolyte solution is sandwiched between two identical electrodes, mimicking the geometry of DSC. The cathode performance is thus investigated under simulated operating conditions of DSC by methods like cyclic voltammetry, chronoamperometry and impedance spectroscopy, but without interference from TiO_2 photoanode. Figure 1 shows the results for pristine graphene oxide (GO) and the same electrode after heat treatment at 450 °C in Ar atmosphere (GO-HT) or after chemical reduction with hydrazine (RGO = reduced graphene oxide). The pristine GO film had T_{550} = 97 %, which decreased to 83 % for GO-HT or 85 % for RGO. This manifested itself by color change from light yellowish (for GO) to gray for RGO and GO-HT. The dummy cells were studied by cyclic voltammetry (top left panel in Figure 1) and by electrochemical impedance spectroscopy (the remaining panels in Figure 1). The GO electrode shows a very poor voltammogram, which reminds that of pure FTO.[20] However, the cyclic voltammograms of RGO and GO-HT confirm dramatic improvement in electrocatalytic activity. They exhibit a plateau limiting current density, j_L of ca. 11.2 mA/cm^2, which is controlled by mass transport in the electrolyte solution

$$jL = 2nFcD/\delta \quad (1)$$

where n = 1 is the number of electrons, F is the Faraday constant, c is concentration, D is the diffusion coefficient, and δ is the distance between electrodes in a dummy cell. The transport-controlling species is $Co(bpy)_3^{3+}$ (c = 50 mmol/L) and δ = 53 μm (see Experimental Section) hence, eq 1 provides the value of $D = 6.2 \times 10^{-6}$ cm^2/s. This is expectedly close to the diffusion coefficient found in the same medium for GNP-electrode.[19] Compared to I-mediated systems, the mass transport is more important for Co-polypyridine redox shuttles. One of the reasons is that the limiting current (eq 1) cannot be increased by concentration, c due to low solubility of Co(III) species.[7,9]

The inverse slope of a voltammogram at the potential of 0 V is the overall cell resistance (R_{CV}) at low overpotentials.[37] The found R_{CV} values are 11 Ωcm^2 or 21 Ωcm^2 for the GO-HT or RGO electrodes, respectively (Figure 1). These resistances are similar to those of GNP-electrodes[19] but an order of magnitude smaller than the resistance reported for a similar Co-bipyridine complex in 3-methoxypropionitrile on an Au-electrode.[37] Nevertheless, in the region of medium overpotentials (between ca. 0.1 to 0.6 V), the GO-HT electrode exhibits less steep voltammogram compared to that of GNP electrode of similar optical density (cf. Figure 1 in ref 19) and the RGO electrode shows even complicated 'two-waves' shape, which will not be discussed here.

Further information about electrocatalytic activity of graphene[38−40] and DSC cathodes[19,20,23,24,26,35,41−43] follows from electrochemical impedance spectroscopy. In our optically transparent electrodes, we can neglect the Nernst diffusion impedance in pores.[23] The reason is that the amount of carbon is too small to exhibit porosity which would be measurable by impedance spectra.[19] The pristine GO film (Figure 1, top right chart) is exceptional by 2−3 orders of magnitude larger impedance than the other electrodes, and we will not analyze it. The remaining two spectra can be fitted to simplified equivalent circuit shown in Figure 2 (model 1)[19,20,24] with R_S = ohmic

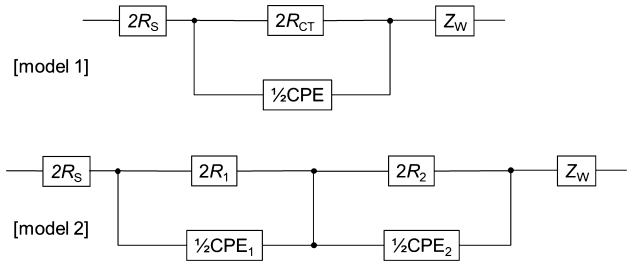

Figure 2. Equivalent circuit diagram for fitting the electrochemical impedance spectra of a dummy cell with two identical electrodes.

serial resistance, Z_W = Nernst diffusion impedance in the bulk electrolyte, and CPE = constant phase element describing deviation from the ideal capacitance, due to the electrode roughness.[35,41−43] Solid lines in our impedance spectra (Figure 1 bottom charts) are the corresponding fits of experimental data to model 1 equivalent circuit (Figure 2). The fits are reasonably good. Our Nyquist plots of impedance spectra would look "compressed" if plotted with the same scaling of $Z'/-Z''$ axes. This shape is quite characteristic for various graphene-based electrodes.[19,20,23,24,26]

The low-frequency semicircles in the spectra of GO-HT and RGO (Figure 1 bottom charts) are diagnostic for mass transfer in the electrolyte solution, expressed as Warburg impedance

$$Z_W = \frac{W}{\sqrt{i\omega}}\tanh\sqrt{\frac{i\omega}{K_N}} \quad (2)$$

(where W is the Warburg parameter and $K_N = D/0.25\delta^2$).[35] The low-frequency semicircle has a similar shape for both the GO-HT and RGO electrodes (Figure 1) as well as for all other active electrodes studied here (vide infra) and in another study employing the same electrolyte solution.[19] This confirms that ionic diffusion in the solution is invariant of the electrode material, provided the latter is active enough. Fitting of low-frequency semicircle to Z_W provides the diffusion coefficient (eq 2) between 2×10^{-6} cm^2/s and 6×10^{-6} cm^2/s, which is in accord with cyclic voltammetry (see above) and similar to the value reported for GNP-electrodes.[19]

The high-frequency semicircle provides the values of R_s, R_{CT}, and Z_{CPE}. The latter element equals:

$$Z_{CPE} = B(i\omega)^{-\beta} \quad (3)$$

where B, β are frequency-independent parameters of the CPE ($0 \leq \beta \leq 1$). For the GO-HT electrode (Figure 1), fitting of the high-frequency semicircle provided the following values: R_s = 1.9 Ωcm^2, R_{CT} = 0.51 Ωcm^2, $B = 6.6 \times 10^{-6}$ Ss$^\beta$, β = 0.97. Analogously for the RGO electrode we fitted: R_s = 1.5 Ωcm^2, R_{CT} = 3.4 Ωcm^2, $B = 2.1 \times 10^{-6}$ Ss$^\beta$, β = 0.97.

A self-evident requirement for good cathode in DSC is that the species generated at the illuminated photoanode (Co(III) or I_3^-) must be reduced at the counterelectrode with comparable speed. This quantifies the exchange current density, j_o to be comparable with photocurrent density on the TiO_2 photoanode. The latter is ca. 20 mA/cm^2 for good cells[3,4] under AM 1.5 solar illumination.[3,4] The exchange current density is

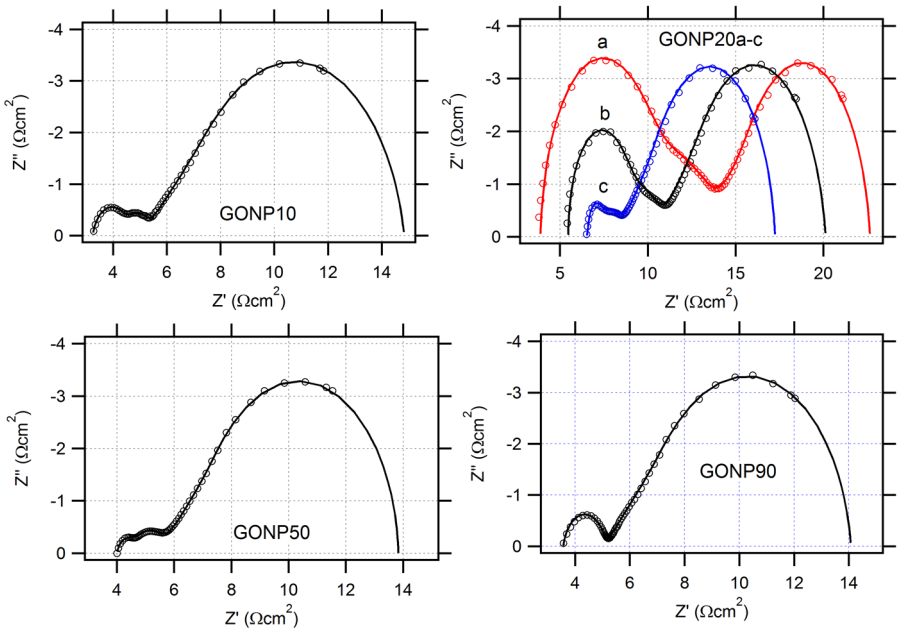

Figure 3. Electrochemical activity of composite electrodes made from graphene oxide and graphene nanoplatelets in various proportions: GONP10 (10% GO; GONP20 (20% GO), GONP50 (50% GO), and GONP90 (90% GO). The data for GONP20 are shown for three different loadings of carbonaceous films. Nyquist plot of electrochemical impedance spectra measured at 0 V from 65 kHz to 0.1 Hz on symmetrical dummy cells. Experimental data (points) were fitted to the equivalent circuits shown in Figure 2 and the fits are displayed as full lines.

simply determined from charge transfer resistance, R_{CT} using the following equation

$$j_0 = \frac{RT}{nFR_{CT}} \quad (4)$$

(where R is the gas constant and T is temperature). Obviously, for j_0 = 20 mA/cm^2, we require R_{CT} = 1.3 Ωcm^2, which is met by our GO-HT, but not by RGO (see above). Trancik *et al.*[44] proposed softer conditions for an all-carbonaceous electrode, which would, eventually, replace Pt-FTO in a dye-sensitized solar cell: R_{CT} of 2−3 Ωcm^2, T_{550} > 80%, and sheet resistance of 20 Ω/sq. However, the electrocatalytic activity, conductivity, and optical transmittance need to be balanced, and an all-carbon electrode meeting all three benchmarks was not yet demonstrated.[28,44,45] We have found an empirical rule, that the j_0 scaled linearly with (−log T_{550}) for GNP films in variety of systems, both Co- and I-mediated.[19,20,24] This pointed at a conclusion that the exchange current density is directly proportional to concentration of catalytically active defects (presumably oxidic groups[23,26]) in carbonaceous film.[19,20,24]

However, this conclusion leaves a debatable issue, that the material with the largest concentration of oxidic functionalities (pristine GO) is exemplary inactive, whereas the GO treated by hydrazine or simply by calcination in inert atmosphere, exhibits strong increase in activity, in spite of the fact that the concentration of oxidic functionalities is known to decrease during both chemical reduction and heat treatment.[46] For our FTO-supported thin films, we cannot argue that oxidized material is handicapped by low conductivity as it was the case of FGS electrodes.[23] The behavior of GO, GO-HT and RGO points at a conclusion that the catalytically active sites are created by irreversible removal of the oxidic functionalities from carbonaceous skeleton rather than by their presence. This finding qualitatively supports the proposal by Velten et al.[47] that the electrocatalytic activity of carbonaceous cathode for DCS is caused by dangling bonds and "sharp atomic edges" in analogy to edge-plane pyrolytic graphite.[34] To further explore this hypothesis, we tested the performance of basal plane highly organized pyrolytic graphite (HOPG) in our dummy cells, and the results are shown in S1 (see the Supporting Information). The basal-plane HOPG electrode is very slow, resembling the properties of GO. Qualitatively, this supports the idea that active sites are at edges of graphene. Our thermally treated graphene oxide shows better electrochemical performance than chemically reduced graphene oxide, which is in accord with earlier studies.[40] Specifically, our GO-HT exhibits by a factor of 7 smaller value of R_{CT} and by a factor of 2 smaller value R_{CV} than the RGO electrode, even though both electrodes have similar optical transmission, T_{550} of 83% or 85% (cf. Figure 1 and discussion thereof). It is tempting to correlate the electrocatalytic activity of GO-HT and RGO with the density of dangling bonds, step edges, and other sharp atomic features,[34,47] but we do not have enough supporting data at this stage of research.

The found parameters of GO-HT electrode are promising, but less good compared to those of pure GNP cathode of similar optical density.[19] For instance, GNP cathode with T_{550} = 85 % exhibited R_{CT} ≈ 0.08 Ωcm^2 and its cyclic voltammogram was more steep than that of GO-HT electrode, as discussed above. To further explore this issue, we have screened composites of GO and GNP in varying proportions for optimization of their catalytic performance. Representative data are summarized in Figure 3, where we show results for composites of GO with GNP containing the following amounts of GO: 10% (GONP10), 20% (GONP20), 50% (GONP50), and 90% (GONP90). All composite electrodes were subjected to heat treatment at 450°C in Ar, as in the case of GO-HT electrode discussed above.

The most interesting feature of composite materials with low proportion of GO is the occurrence of two high-frequency semicircles in impedance spectra, instead of one semicircle

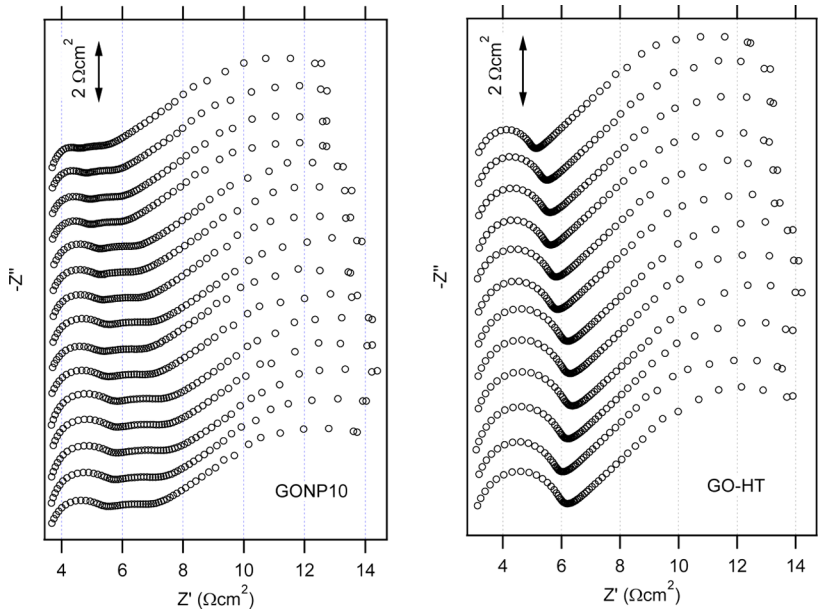

Figure 4. Stability test by electrochemical impedance spectra on symmetrical dummy cell. The top curve is for freshly assembled dummy cell and each next curve towards bottom was measured after one day of aging. Before each measurement, the cell was subjected to one cyclic voltammetry scan (from 0 V → 1 V → −1 V → 0 V, scan rate 50 mV/s) followed by 20 s relaxation at 0 V, followed by electrochemical impedance measurement at 0 V from 65 kHz to 0.1 Hz. Data are shown for graphene oxide/nanoplatelets composite electrode, GONP10 (10% GO) and for pure heat-treated graphene oxide (GO-HT). Impedance spectra are offset in the $-Z''$ scale for better visualization.

present in the spectra of pure GNP-electrodes,[19,20] GO-HT and RGO electrodes (Figure 1). The spectra of GONP10, GONP20, and GONP50 can be fitted to equivalent circuit in model 2, Figure 2. The doublet of high-frequency semicircles is found independently of the carbon film loading; an example is shown in Figure 3 (top right chart) for three different GONP20 electrodes (with T_{550} equal to 95, 88, and 78% for spectra a, b and c, respectively). The serial combination of two RCPE elements in model 2 (Figure 2) is rationalized by a hypothesis that the composite material has two distinct subunits: one directly interacting with FTO surface: R_1CPE_1 (presumably GO-based) and the other, R_2CPE_2 (presumably GNP-based) is anchored to it in series. Solely in the case of GONP90, the experimental data can be again fitted to model 1 (Figure 2) circuit with reasonable accuracy. This particular electrode (T_{550} = 83%) provided the fitted value of R_{CT} = 0.78 Ωcm^2 which is again considerably larger than the value for pure GNP of similar optical density,[19] but obviously acceptable for DSC application (cf. eq 4 and discussion thereof). The optimum material is GONP50 (T_{550} = 90%) with fitted values R_1 = 0.23 Ωcm^2 and R_2 = 0.38 Ωcm^2. This is the best charge-transfer resistance for such a low carbon mass loading (high optical density) from all our electrodes tested.

Electrochemical stability of our electrodes was studied by repeated measurements of electrochemical impedance after certain time of aging at room temperature and open circuit. (Before each measurement of impedance spectrum, the dummy cell was subjected to one short voltammetric scan, see the Experimental Section). Figure 4 shows the representative data for GONP10 and GO-HT electrodes. The top curve is for a freshly assembled dummy cell and each next curve towards bottom is the spectrum reproduced after one day of aging. (The spectra are offset in the $-Z''$ scale for better visualization.) Earlier studies of GNP-electrodes revealed considerable sensitivity to aging in this medium: the charge transfer resistance of GNP increased from R_{CT} < 0.08 Ωcm^2 to 0.2 Ωcm^2 during 14 days of storage.[19] Similar aging effect was noticed for GNP-electrode in $[Co(bpy\text{-}pz)_2]^{3+/2+}$ electrolyte solution.[20]

Our GO-based electrodes (Figure 4) also show some activity loss, expressed as increase of the high-frequency semicircle(s) with time of aging. However, the growth of R_{CT} is slower than that of GNP-electrodes.[19,20] The actual GO-HT electrode in Figure 4 had R_{CT} = 0.82 Ωcm^2 in freshly made dummy cell; this value increased to 0.99 Ωcm^2 during the first day, subsequently to 1.39 Ωcm^2 after 8 days, but dropped again to 1.27 Ωcm^2 after 11 days. Screening of various other dummy cells confirmed that the growth of R_{CT} seems to stop after ca. 6−10 days of aging (cf. also S2 in the Supporting Information). This effect is characteristic for GO-based electrodes; it was not observed for GNP-electrodes.[19,20] After the initial period of 6−10 days, the spectra of GO-based electrodes show fluctuations which may account for experimental error, rather than for progressive aging anymore. We regularly observed that the aging was more pronounced for materials with (i) smaller carbon loading (higher T_{550}), and (ii) higher proportion of GNP in the composite (such as GONP10, cf. Figure 4). This effect is further illustrated by analogous plot for GONP90 (S2 in the Supporting Information).

The aging of DSC cathodes is quite often ignored in works dealing with screening and optimization of electrode materials (with few exceptions represented by refs 6, 19, 20, 24, 35, 48, and 49). This aging, also termed "poisoning" is present even in the classical I-mediated DSC with Pt cathode.[24,35,49] It does not seem to be detrimental for proper function of DSC, as documented by the long-term stability of practical devices.[5] Although detailed experimental evidence is missing, we assume that aging of Pt in I-mediated systems may stop after some initialization period similarly to the behavior of GO-based electrodes. Surprisingly, the pristine GO electrode shows aging too, but with the opposite trend: instead of increasing, the impedance drops considerably during days of contact with the

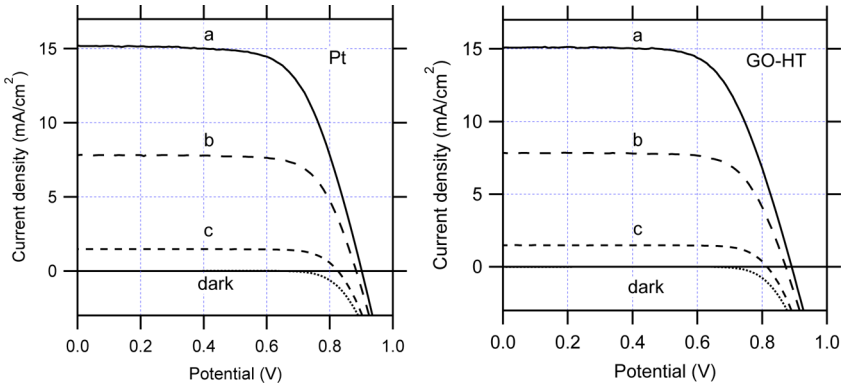

Figure 5. Current–voltage characteristics of dye sensitized solar cells with Y-123 sensitized TiO_2 photoanode in acetonitrile solution of $Co(bpy)_3^{3+/2+}$. Left chart is for DSC with Pt-cathode; right chart is for DSC with GO-HT cathode (T_{550} = 86%). The illumination intensity is 1 sun (curves a), 0.51 sun (curves b), 0.095 sun (curves c), and 0 (curves dark).

electrolyte solution. We have no explanation for this phenomenon; but speculate that some irreversible reorganization of graphene oxide could take place at the interface in situ.

Finally, we tested the performance of our counterelectrodes in $Co(bpy)_3$-mediated solar cells with Y123-sensitized TiO_2 photoanodes. (For the chemical formula of Y123 see Scheme S4 in the Supporting Information). We used the same DSC fabrication protocol as in our earlier communication on GNP-cathodes[19] to facilitate comparison. Figure 5 shows representative current-voltage characteristics under simulated solar irradiation for DSCs with GO-HT cathode and Pt-cathode. We should note that our reference solar cell with Pt-cathode (Figure 5 left chart) exhibited somewhat better performance than that used in earlier work.[19] It is most likely ascribed to optimized thickness of the active layer of TiO_2 photoanode (5.5 μm, see Experimental Section) which is larger by about 20% compared to previous study.[19]

Our GO-based electrodes do not show the problem with enhanced dark current anymore, which was previously identified as one of the explicit drawbacks of GNP-electrodes.[19] All our electrodes exhibit dark current, which is identical to that for Pt-counterelectrode, within experimental errors. For instance, the dark current for DSC with a Pt-cathode is ~0.6 mA/cm^2 at 0.8 V (Figure 5; cf. also Figure S6 in ref 19). A similar value is observed for a DSC with GO-HT cathode (Figure 5) and for all other GO-based cathodes investigated here (data not shown). Note that the pure GNP-cathode exhibited dark current of ca. 1.4 mA/cm^2 at 0.8 V (Figure S5 in ref 19). Blocking of dark current in GO-based electrodes can be explained by improved film structure and firm bonding to FTO, which prevents peeling of carbonaceous particles from the cathode, and their subsequent deposition on the photoanode.[19,26]

Table S1 (see the Supporting Information) collects detailed parameters of various solar cells tested in this work. In terms of solar conversion efficiency, all our systems behave similarly. This confirms the conclusion from impedance spectroscopy, that all our counterelectrodes are sufficiently active to provide the requested exchange current density (see eq 4 and discussion thereof). The differences between individual devices with various cathodes are rather statistical than systematic. We do not trace any clear trends, except, perhaps, for slightly larger currents, but smaller voltages for most DSCs with GO-based cathodes compared to DSC with Pt-cathode. Obviously, the solar cells with GO-based cathodes compare satisfactorily to the performance of DSC with Pt counterelectrode. In summary, electrode materials based on graphene oxide are strong candidates to avoid platinum in the next generation of solar cells using Co-mediators.

3. CONCLUSION

We developed a new fabrication protocol towards graphene-based cathodes for optically transparent dye sensitized solar cells. The active electrode material was prepared from single-layer graphene oxide either pure or in a composite with graphene nanoplatelets. Compared to films from pure graphene nanoplatelets, the GO-based electrodes showed better mechanical and electrochemical stability, but without any significant drop in electrocatalytic activity for $Co(bpy)_3^{3+/2+}$. Impedance spectra of GO/GNP composites exhibited specific features, which were ascribed to two distinguishable electrocatalytic subunits in series. The aging-induced loss of activity was smaller for GO-based electrodes compared to that in GNP-electrodes.

The electrocatalytic activity towards $Co(bpy)_3^{3+/2+}$ redox reaction was found to be considerably better for thermally treated graphene oxide referenced to that of chemically (by hydrazine) reduced graphene oxide of comparable optical transmittances. Still better electrochemical performance was found for heat-treated composites from graphene oxide and graphene nanoplatelets; the optimum electrode material contained 50% of graphene oxide and 50% of graphene nanoplatelets (GONP50).

The good electrochemical performance of GO-containing films is applicable for dye-sensitized solar cells with Y123-sensitized TiO_2 photoanodes and $Co(bpy)_3^{3+/2+}$ as the redox shuttle. The efficiency of solar cells with GO-based cathodes compared satisfactorily to the efficiency of solar cells with Pt counterelectrode.

We collected here further arguments for the ongoing discussion of electrocatalytic activity of carbons in general and nanocarbons in particular. The sole presence of oxidic functional groups on carbonaceous skeleton is not decisive for electrocatalysis. This was demonstrated by the behavior of pristine GO which shows almost no activity, resembling the basal plane pyrolytic graphite, but improves dramatically upon chemical reduction of GO with hydrazine and/or heat treatment. Presumably, the electrocatalytic activity is promoted by dangling bonds at graphene edges, which are formed in this way.

4. EXPERIMENTAL SECTION

Materials and Preparation of Electrodes. Single-layer graphene oxide (GO) and graphene nanoplatelets (GNP), Grade 3 were purchased from Cheap Tubes, Inc. (USA). According to the manufacturer's specification, the GNP nanoplatelets consisted of several sheets of graphene with an overall thickness of approximately 5 nm (ranging from 1 nm to 15 nm), particle diameters less than 2 micrometers and surface area of 600−750 m^2/g. GO was dissolved in water by short sonication to form solutions with concentration 1-10 mg/mL. The platelets were dispersed in water by sonication (ca. 1 minute) and the solution was left overnight to separate larger particles by sedimentation. The supernatant dispersion containing about 1 mg/mL was stable for several days without marked sedimentation. Precursor for composite electrodes was prepared by mixing this dispersion with GO solution to a desired proportion of GO/GNP. FTO glass (TEC 15 from Libbey-Owens-Ford, 15 Ohm/sq) was cleaned by the so-called piranha solution (3:1 mixture of 96 % H_2SO_4 and 30 % H_2O_2). Sometimes, FTO glass was cleaned ultrasonically in isopropanol followed by treatment in UVO-Cleaner (model 256-220, Jelight Co., Inc.). Better quality films were usually fabricated on piranha-treated FTO glass. The films were deposited from aqueous solutions by (i) drop-casting, (ii) air-brush spraying, or (iii) spin coating. Drop casting provided non-uniform layers, hence the other two techniques are preferable. For practical reasons such as easy scaling up, the spraying over a warm substrate (ca. 100°C) was used preferably in this work. The amount of deposited carbon was adjusted by the time of spraying, and was quantified by measurement of optical density. Consistent with our previous works,[19,20,24] the optical transmittance at a wavelength of 550 nm, T_{550} served as a parameter characterizing all films. Some electrodes were subsequently annealed in Ar atmosphere at 450°C for 1 h. Chemical reduction of GO film was carried out by treatment with a vapor of hydrazine monohydrate (Aldrich) at 40°C overnight following the recipe detailed in Ref.[46] Thus prepared reduced graphene oxide (RGO) was purified from N_2H_4 by heating at 120°C in air. Platinized FTO (Pt-FTO) was prepared by deposition of 5 $\mu L/cm^2$ of 10 mM H_2PtCl_6 in 2-propanol and calcination at 400°C for 15 minutes. HOPG (graphite monochromator, grade ZYB) was purchased from Momentive Performance Materials Quartz, Inc. (USA). The electrodes were prepared by peeling off the HOPG block using the double-sided adhesive Scotch tape. The film was deposited on glass and contacted by silver paint.

The symmetrical sandwich dummy cell was fabricated from two identical FTO sheets which were separated by Surlyn (DuPont) tape as a seal and spacer. The cell was assembled by thermal melting of Surlyn leaving 0.6 × 0.6 cm^2 active area. The sheet edges were coated by ultrasonic soldering (Cerasolzer alloy 246, MBR Electronics GmbH) to improve electrical contacts. The distance between electrodes was measured by a digital micrometer, and the average value was (53 ± 5) μm. To present comparable electrochemical data, avoiding small sample-to-sample variations in cell thicknesses, we corrected the measured current densities in cyclic voltammograms and chronoamperometric plots by a coefficient of $53/\delta_G$, where δ_G is the measured thickness (in μm) of the actual dummy cell. The cell was filled with an electrolyte through a hole in one FTO support, which was finally closed by a Surlyn seal. The electrolyte solution was 0.22 M $Co(bpy)_3(B(CN)_4)_2$, 0.05 M $Co(bpy)_3(B(CN)_4)_3$, 0.1 M $LiClO_4$, and 0.2 M 4-*tert*-butylpyridine in acetonitrile. The dummy cell with HOPG was fabricated in a similar way, but the thickness of Surlyn spacer was doubled to avoid short-circuit through the electrode and/or silver contacts. In this case, the cell was not sealed thermally, but only mechanically tightened by a clip, and electrolyte was filled through a hole in Surlyn spacer.

Photoelectrochemical tests were carried out with TiO_2 films composed of 20 nm diameter anatase nanoparticles. The TiO_2 transparent films were deposited by screen printing onto fluorine-doped tin oxide (FTO, Solar 4 mm thickness, 10 ohms per sq, Nippon Sheet Glass) conducting glass. Around 5.5 μm film was obtained by the number of screen-printing cycles and a ∼5 μm scattering layer (400 nm diameter, Catalysts & Chemicals Ind. Co. Ltd. (CCIC), HPW-400) was deposited on the transparent layer. The TiO_2 electrode was sensitized with 3[6-[4-[bis(2′,4′-dihexyloxybiphenyl-4-yl)amino-]phenyl]-4,4-dihexyl-cyclopenta-[2,1-b:3,4-b′]dithiophene-2-yl]-2-cyanoacrylic acid, coded Y123 by overnight dipping into 0.1 mM solution of the dye in 4-*tert*-butanol/acetonitrile mixture (1:1 v/v). The DSC was assembled with a counterelectrode using a Surlyn tape (25 μm in thickness) as a seal and spacer (see above). The cell active area for illumination was 0.2 cm^2, defined by a light-shading mask. A self-adhesive, anti-reflecting, ultraviolet cutoff film (λ < 380 nm, ARKTOP, ASAHI Glass) was attached to the top of active area to decrease light reflection loss.

Methods. Electrochemical measurements were carried out using a PAR 273 potentiostat (EG&G) interfaced to a Solartron 1260A frequency response analyzer and controlled by a CorrWare program. Electrochemical impedance data were processed using Zplot/Zview software. The impedance spectra were acquired in the frequency range from 65 kHz to 0.1 Hz, at 0 V bias voltage, the modulation amplitude was 10 mV. Before each measurement of impedance spectrum, the dummy cell was subjected to one fast voltammetric scan (between −1 and 1 V, 50 mV/s) followed by 20 s relaxation at 0 V. The optical spectra were measured by Varian Cary 5 spectrometer with integrating sphere in transmission mode. Blank FTO sheet served as a reference. For photoelectrochemical tests, the light source was a 450 W xenon light source (Osram XBO 450, Germany) with a filter (Schott 113). The light power was regulated to the AM 1.5G solar standard by using a reference Si photodiode equipped with a color-matched filter (KG-3, Schott) to reduce the mismatch between the simulated light and AM 1.5G to less than 4% in the wavelength region of 350−750 nm. The differing intensities were regulated with neutral wire mesh attenuator. The applied potential and cell current were measured using a Keithley model 2400 digital source meter.

■ ASSOCIATED CONTENT

Ⓢ Supporting Information

Electrochemical activity of HOPG, stability test by electrochemical impedance spectra of GONP90 and GO electrodes, structural formula of Y123, and table of detailed solar cells characteristics. This material is available free of charge via the Internet at http://pubs.acs.org/.

■ AUTHOR INFORMATION

Corresponding Author

*E-mail: kavan@jh-inst.cas.cz.

Notes

The authors declare no competing financial interest.

■ ACKNOWLEDGMENTS

This work was supported the Academy of Sciences of the Czech Republic (Contracts IAA 400400804 and KAN 200100801) and by the FP7-Energy-2010-FET project Molesol (Contract 256617). Partial support of this work by NEC Corporation, Japan is also acknowledged. MG is very grateful to the European Research Council (ERC) for supporting his research under the ERC-2009-AdG Grant 247404 MESO-LIGHT. JHY acknowledges the support from the Korea Foundation for International Cooperation in Science & Technology through the Global Research Lab. The authors thank Mr. Pascal Comte, Dr. Yongjoo Kim, and Dr. Florian Kessler for their kind assistance in preparing the TiO_2 paste, the TiO_2 films, and the cobalt complex. The authors also thank NEC corporation (Japan) for providing the Y123 dye.

■ REFERENCES

(1) Grätzel, M. *Nature* **2001**, *414*, 338−344.
(2) O'Regan, B.; Grätzel, M. *Nature* **1991**, *353*, 737−740.

(3) Hagfeldt, A.; Boschloo, G.; Sun, L.; Kloo, L.; Pettersson, H. *Chem. Rev.* **2010**, *110*, 6595−6663.
(4) Hardin, B.E.; Snaith, H.J.; McGehee, M.D. *Nat. Photonics* **2012**, *6*, 161−169.
(5) Kalyanasundaram,K.*Dye Sensitized Solar Cells*; CRC Press Taylor & Francis: Boca Raton, FL, 2010.
(6) Gong, F.; Wang, H.; Xu, X.; Zhou, G.; Wang, Z.S. *J. Am. Chem. Soc.* **2012**, *134*, 10953−10958.
(7) Hamann, T.W.; Ondersma, J.W. *Energy Environ. Sci.* **2011**, *4*, 370−381.
(8) Wu, M.; Lin, X.; Wang, L.; Guo, W.; Qi, D.; Peng, X.; Hagfeldt, A.; Grätzel, M.; Ma, T. *J. Am. Chem. Soc.* **2012**, *134*, 3419−3428.
(9) Hamann, T.W. *Dalton Trans.* **2012**, *41*, 3111−3115.
(10) Cong, J.; Yang, X.; Kloo, L.; Sun, L. *Energy Environ. Sci.* **2012**, DOI: 10.1039/c2ee22095d.
(11) Tsao, H.N.; Burschka, J.; Yi, C.; Kessler, F.; Nazeeruddin, M.K.; Grätzel, M. *Energy Environ. Sci.* **2011**, *4*, 4921−4924.
(12) Ahmad, S.; Bessho, T.; Kessler, F.; Baranoff, E.; Frey, J.; Yi, C.; Grätzel, M.; Nazeeruddin, M.K. *Phys. Chem. Chem. Phys.* **2012**, *14*, 10631−10639.
(13) Feldt, S.M.; Gibson, E.A.; Gabrielsson, E.; Sun, L.; Boschloo, G.; Hagfeldt, A. *J. Am. Chem. Soc.* **2010**, *132*, 16714−16724.
(14) Tsao, H.N.; Yi, C.; Moehl, T.; Yum, J.-H.; Zakeeruddin, S.M.; Nazeeruddin, M.K.; Grätzel, M. *ChemSusChem* **2011**, *4*, 591−594.
(15) Zhou, D.; Yu, Q.; Cai, N.; Bai, Y.; Wang, Y.; Wang, P. *Energy Environ. Sci.* **2011**, *4*, 2030−2034.
(16) Liu, J.; Zhang, J.; Xu, M.; Zhou, D.; Jing, X.; Wang, P. *Energy Environ. Sci.* **2011**, *4*, 3021−3029.
(17) Yum, J.-H.; Baranoff, E.; Kessler, F.; Moehl, T.; Ahmad, S.; Bessho, T.; Marchioro, A.; Ghadiri, E.; Moser, J.E.; Nazeeruddin, M.K.; Grätzel, M. *Nat. Commun.* **2012**, *3*, 631−6318.
(18) Yella, A.; Lee, H.W.; Tsao, H.N.; Yi, C.; Chandiran, A.K.; Nazeeruddin, M.K.; Diau, E.W.G.; Yeh, C.Y.; Zakeeruddin, S.M.; Grätzel, M. *Science* **2011**, *334*, 629−634.
(19) Kavan, L.; Yum, J.-H.; Grätzel, M. *Nano Lett.* **2011**, *11*, 5501−5506.
(20) Kavan, L.; Yum, J.-H.; Nazeeruddin, M.K.; Grätzel, M. *ACS Nano* **2011**, *5*, 9171−9178.
(21) Sapp, S.A.; Elliot, M.; Contado, C.; Caramori, S.; Bignozzi, C.A. *J. Am. Chem. Soc.* **2002**, *124*, 11215−11222.
(22) Ghamouss, F.; Pitson, R.; Odobel, F.; Boujtita, M.; Caramori, S.; Bignozzi, C.A. *Electrochim. Acta* **2010**, *55*, 6517−6522.
(23) Roy-Mayhew, J.D.; Bozym, D.J.; Punckt, C.; Aksay, A. *ACS Nano* **2010**, *10*, 6203−6211.
(24) Kavan, L.; Yum, J.-H.; Grätzel, M. *ACS Nano* **2011**, *5*, 165−172.
(25) Lee, J.S.; Ahn, H.J.; Yoon, J.C.; Jang, J.H. *Phys. Chem. Chem. Phys.* **2012**, *14*, 7938−7943.
(26) Roy-Mayhew, J.D.; Boschloo, G.; Hagfeldt, A.; Aksay, I.A. *ACS Appl. Mater. Interfaces* **2012**, *4*, 2794−2800.
(27) Yeh, M.H.; Sun, C.L.; Su, J.S.; Lin, J.Y.; Lee, C.P.; Chen, C.Y.; Wu, C.G.; Vittal, R.; Ho, K.C. *Carbon* **2012**, *50*, 4192−4202.
(28) Lee, B.; Buchholz, D.B.; Chang, R.P.H. *Energy Environ. Sci.* **2012**, *5*, 6941−6952.
(29) Choi, H.; Kim, H.; Hwang, S.; Han, Y.; Jeon, M. *J. Mater. Chem.* **2011**, *21*, 7548−7551.
(30) Kim, H.; Choi, H.; Hwang, S.; Kim, Y.; Jeon, M. *Nanoscale Res. Lett.* **2012**, *7*, 53−534.
(31) Choi, H.; Hwang, S.; Bae, H.; Kim, S.; Kim, H.; Jeon, M. *Electron. Lett.* **2011**, *47*, 281−283.
(32) Zhang, D.W.; Li, X.D.; Li, H.B.; Chen, S.; Sun, Z.; Yin, X.J.; Huang, S.M. *Carbon* **2011**, *49*, 5382−5388.
(33) Dubacheva, G.V.; Liang, C.K.; Bassani, D.M. *Coord. Chem. Rev.* **2012**, *256*, 2628−2639.
(34) Pumera, M. *Chem.—Eur. J.* **2009**, *15*, 4970−4978.
(35) Hauch, A.; Georg, A. *Electrochim. Acta* **2001**, *46*, 3457−3466.
(36) Tung, V.C.; Huang, J.H.; Tevis, I.; Kim, F.; Kim, J.; Chu, C.W.; Stupp, S.I.; Huaong, J. *J. Am. Chem. Soc.* **2011**, *133*, 4940−4947.
(37) Liberatore, M.; Petrocco, A.; Caprioli, F.; La Mesa, C.; Decker, F.; Bignozzi, C.A. *Electrochim. Acta* **2010**, *55*, 4025−4029.
(38) Chua, C.K.; Sofer, Z.; Pumera, M. *Chem.—Eur. J.* **2012**, *18*, 13453−13459.
(39) Bonanni, A.; Pumera, M. *Electrochem. Comm.* **2013**, *26*, 52−54.
(40) Ambrosi, A.; Bonanni, A.; Sofer, Z.; Cross, J.S.; Pumera, M. *Chem.—Eur. J.* **2011**, *17*, 10763−10770.
(41) Murakami, T.N.; Ito, S.; Wang, Q.; Nazeeruddin, M.K.; Bessho, T.; Cesar, I.; Liska, P.; Humphry-Baker, R.; Comte, P.; Pechy, P.; Grätzel, M. *J. Electrochem. Soc.* **2006**, *153*, A2255−A2261.
(42) Liberatore, M.; Decker, F.; Burtone, L.; Zardetto, V.; Brown, T.M.; Reale, A.; Di Carlo, A. *J. Appl. Electrochem.* **2009**, *39*, 2291−2295.
(43) Wang, G.; Xing, W.; Zhou, S. *J. Power Sources* **2009**, *194*, 568−573.
(44) Trancik, J.E.; Barton, S.C.; Hone, J. *Nano Lett.* **2008**, *8*, 982−987.
(45) Tantang, H.; Kyaw, A.K.K.; Zhao, Y.; Park, M.B.C.; Tok, A.I.Y.; Hu, Z.; Li, L.J.; Sun, X.W.; Zhang, Q. *Chem. Asian J.* **2012**, *7*, 51−545.
(46) Becerril, H.A.; Mao, J.; Liu, Z.; Stoltenberg, R.M.; Bao, Z.; Chen, Y. *ACS Nano* **2008**, *2*, 463−470.
(47) Velten, J.; Mozer, A.J.; Li, D.; Officer, D.; Wallace, G.; Baughman, R.H.; Zakhidov, A.A. *Nanotechnology* **2012**, *23*, 085201−0852016.
(48) Wu, M.; Lin, X.; Wang, Y.; Wang, L.; Guo, W.; Qi, D.; Peng, X.; Hagfeldt, A.; Grätzel, M.; Ma, T. *J. Am. Chem. Soc.* **2012**, *134*, 3419−3428.
(49) Olsen, E.; Hagen, G.; Lindquist, S.E. *Solar Energy Mater. Sol. Cells* **2000**, *63*, 267−273.